IEEE Access
Multidisciplinary | Rapid Review | Open Access Journal

Received January 15, 2020, accepted February 10, 2020, date of publication February 17, 2020, date of current version March 3, 2020.

Digital Object Identifier 10.1109/ACCESS.2020.2974247

No Load Simulation and Downscaled Experiment of UHV Single-Phase Autotransformer Under DC Bias

BING LI, ZEZHONG WANG, SUXIN GUO, AND MINGYANG LI

State Key Laboratory of Alternate Electrical Supply System With Renewable Energy Sources, North China Electric Power University, Beijing 102206, China

Corresponding author: Bing Li (ncepu_lb@163.com)

This work was supported in part by the National Key Research and Development Program of China under Grant 2016YFC0800100.

ABSTRACT The time-domain field-circuit coupled finite element method (FEM) is widely used to analyze the DC effects on transformers. However, the long transient process of calculation will encounter difficulties due to the tremendous requirement of computer memory and CPU time, especially when it comes to ultra-high-voltage (UHV) autotransformers, which has a large time constant due to their less resistance and larger inductance. Besides, compared to the AC voltage, the DC voltage is much smaller, miscalculations usually occur as the component of DC bias can be easily neglected in the simulation. In this paper, a time-domain field-circuit coupling FEM combined with the series resistance and voltage compensation method (SRVCM) is proposed, a large resistance is in series in the circuit model to speed up the convergence of transient process and amplify DC component. Afterwards, the voltage supply is increased to compensate for the reduced voltage drop due to series resistance. The excitation waveform and its frequency characteristics of UHV autotransformer under various DC bias are discussed under no-load condition. Its advantages over conventional decrease the numerical miscalculation and the iterations calculation of the transient process. An experimental verification of the proposed method is carried out by a downscaled autotransformer.

INDEX TERMS UHV autotransformer, DC bias, field-circuit coupling finite element method, series resistance and voltage compensation method, downscaled experiment.

I. INTRODUCTION

The increasing global demand for energy consumption and environmental impact become increasingly prominent, the serious energy crisis is becoming a key focus worldwide [1]–[3]. Thus, eight 1000-kV ultra-high voltage (UHV) AC power transmission projects have been put into operation in China and over 100 units of UHV transformers have been put into service for solving the energy crisis [4]. UHV transformer is one of the key equipment of UHV transmission system, their safe and stable operation is directly related to the safety of UHV transmission system. UHV transformers mostly use self-coupling structure, and the transformer group composed of the single-phase autotransformer has less tolerance to the DC bias current [5].

DC bias of transformers is an abnormal working condition. The main causes of DC bias current flowing in transformer windings are mainly from monopole operation of HVDC transmission [6], nonlinear loads such as AC drives, switch-mode power supplies and grid-connected converters, which can cause, the generation of unwanted current harmonics and a DC current component injection into the grid [7], and geomagnetically induced current (GIC) caused by solar magnetic storms, which could attain up to 100 A per phase for 1 min and 50 A per phase for 5 min during the most severe magnetic storm [8]. The main effect of a DC current flowing into a transformer windings is the asymmetric magnetic core saturation during a sinusoidal half-period (half-cycle saturation), as a result, a series of problems occur, such as the serious distortion of excitation current, increased reactive power absorption, partial overheating and increase of vibration and noise [4], [9]–[14]. Thus, precise and in-depth analysis of DC bias for UHV autotransformers is necessary for the safe operation of equipment and transmission systems.

Nowadays, many in-depth research and analysis have been studied on the DC bias problems of transformers by simulations. FEM are wildly used in the analysis of simulations [15]–[21]. However, FEM for the simulation can be

The associate editor coordinating the review of this manuscript and approving it for publication was Mehmet Alper Uslu.

extremely time-consuming with the massive mesh and long transient process, especially in the calculation of UHV autotransformer, consists of large inductance and small resistance, which means a bigger time constant and longer transient process. Due to the large inductance to small resistance as well as the large 1000 kV AC voltage to small DC component in UHV autotransformer, a long transient process of the minimal time step and error criterion is required for avoiding miscalculation by conventional calculation. Although there are many proposed algorithms to shorten the calculation time of FEM, it still needs hours even days to solve the large capacity transformers [22], not mention the DC bias condition, and some research has a really district standard to set up an initial value, which may not suitable for other models [23].

For the purpose of increasing the calculation accuracy and speeding up the convergence of the transient process, this paper proposes a new fast solution by making good use of series resistance and voltage compensation method (SRVCM) based on time-domain filed-circuit coupling FEM. By using this method, (i) we can shorten the transient process and obtain the precise value with acceptable time and memory consumption. (ii) The excitation current waveform, its frequency characteristics and flux distribution of UHV autotransformer without load under DC bias are analyzed, respectively. (iii) An experimental verification of the proposed method is carried out by a downscaled autotransformer.

II. COMPUTATION MODEL COMBINED WITH SRVCM

Nowadays, the time-domain field-circuit coupling FEM is wildly used to calculate electromagnetic quantities of transformer. Based on the time-domain field-circuit coupling model, the electromagnetic calculation of the transformer is divided into field and circuit model, which can obtain dynamic inductance and transient current, respectively.

In order to reduce the transient process, a large series resistance is utilized in the circuit model to reduce the time constant of UHV autotransformer and shorten the transient process. At the same time, voltage compensation is used to make up the voltage drop caused by series resistance, which ensures the winding voltages are consistent with the rated voltage.

A. FIELD-CIRCUIT COUPLING MODEL WITH SERIES RESISTANCE

The capacity of UHV autotransformer has reached 1000 MVA, single-phase four-limb or single-phase five-limb are mainly adopted. This paper focuses on single-phase four-limb UHV autotransformer, which consists of two main limbs and two side limbs. There are low voltage winding, common winding and series winding from inside to outside, respectively. It has to be noted that the tank, the tie bars and the clamping plate which are made of massive steel and carry eddy currents are neglected. The core and the tank shielding are laminated and are assumed to be free of eddy currents. The eighth magnetic model is shown in Fig. 1 (a).

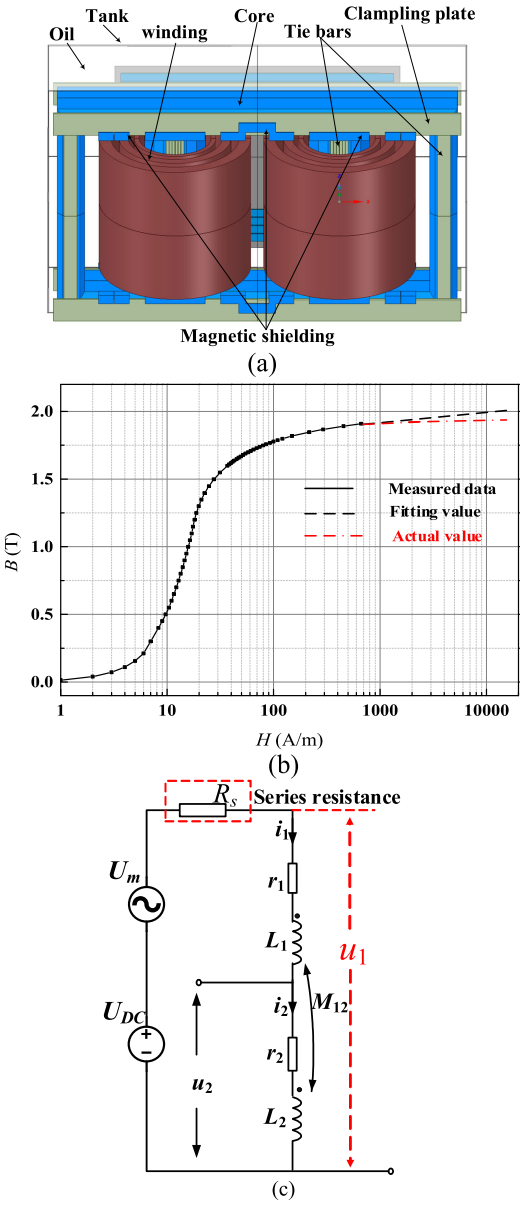

FIGURE 1. Field-circuit coupling model of UHV autotransformer. (a) Model of UHV transformer. (b) B-H magnetization curve. (c) Circuit model with series resistance.

The B-H curve of the core used in the calculation is shown in Fig. 1 (b). It should be noted that the measured data are only provided to 1.91 T, the linear curve fitting method is used to extend the curve. Thus, the actual results are more saturated than the simulation under DC bias. The magnetic field based on the edge FEM is utilized for its good accuracy of boundary problem of high permeability material [24]. The edge FEM differential equation uses vector magnetic potential A and field equation according to Maxwell is as follows

$$\nabla \times \frac{1}{\mu} \nabla \times \boldsymbol{A} = \boldsymbol{J} \tag{1}$$

where μ is permeability of magnetic material, A is vector magnetic potential, $\boldsymbol{J}$ is current density.

Edge element interpolation function can be expressed as

$$\boldsymbol{A} = \sum_{k=1}^{n_n} M_n(x, y, z)\, \boldsymbol{A}_n \tag{2}$$

where $\{M_n, k=1, 2, \ldots, n\}$ is weight function sequences, n is the number of base function sequence, n_n is the total number of edge.

Applying the Green theorem, the Galerkin weighted residual equation is

$$\iiint_V \frac{1}{\mu}(\nabla \times M_m)(\nabla \times M_n)\boldsymbol{A}_n \mathrm{d}V = \iiint_V M_n \boldsymbol{J}\, \mathrm{d}V \tag{3}$$

where M_m is weight function sequences which is the same as basis function, with the known current density $\boldsymbol{J}$, which is supposed to be obtained by circuit model, magnetic vector $\boldsymbol{A}$ can be calculated by substituting the weight function in (3).

In order to accurately calculate the variation of excitation current, the dynamic inductance parameters (the slope of the BH curve) of winding coil are needed to reflect the saturation degree of core while calculating the field-circuit coupling model of DC bias problem. The voltage of dynamic inductance u_L can be obtained by

$$u_L = \frac{d\psi}{dt} = \frac{d\psi}{di}\frac{di}{dt} = L\frac{di}{dt} \tag{4}$$

where ψ is coil flux linkage, i is winding current, L is dynamic inductance.

According to the principle of the disturbance energy, the magnetic field energy change can be expressed as

$$\Delta W_1 = \frac{1}{2}\int \Delta \boldsymbol{B} \cdot \Delta \boldsymbol{H}\, \mathrm{d}V \tag{5}$$

The magnetic field energy changes in the transformer with winding current changes Δi is shown as

$$\Delta W_2 = \frac{1}{2} L \Delta i_m \Delta i_n, \quad (m, n = 1, 2, 3) \tag{6}$$

Based on the principle of energy conservation, $\Delta W_1 = \Delta W_2$, the dynamic inductance L can be obtained.

The circuit diagram with a series resistance is shown in Fig. 1 (c), and the transient differential equations of the circuit model is shown as follows

$$u_{ACi} + u_{DCi} = \sum\nolimits_{ij} (R + r_i) i_i + L_{ii}\frac{\mathrm{d}i_1}{dt} + M_{ij}\left(\frac{\mathrm{d}i_i}{dt} + \frac{\mathrm{d}i_j}{dt}\right) \tag{7}$$

where u_{AC} and u_{DC} are AC and DC voltage, respectively, R is series resistance, L and M present the dynamic self and mutual inductance, respectively.

The fourth-order Runge-Kutta method is selected as the numerical method to solve the voltage differential equation obtained in the field-circuit coupling method. The classical fourth-order Runge-Kutta formula is shown as

$$\begin{cases} i_{k+1} = i_k + \dfrac{h}{6}(K_1 + 2K_2 + 2K_3 + K_4) \\ K_1 = f(x_k, y_k) \\ K_2 = f\left(x_k + \dfrac{h}{2}, y_k + \dfrac{h}{2}K_1\right) \\ K_3 = f\left(x_k + \dfrac{h}{2}, y_k + \dfrac{h}{2}K_2\right) \\ K_4 = f(x_k + h, y_k + hK_3) \end{cases} \tag{8}$$

where h is time step size $K_1 \sim K_4$ are the four slope in a time step, i_k and i_{k+1} are the current values at time t_k and t_{k+1}.

In conclusion, the steps of the non-linear magnetic field with time-domain field-circuit coupling FEM are as follows:

(i) Input coil current i_k to the transformer magnetic field model, based on edge FEM energy disturbance principle, dynamic inductance L can be calculated.

(ii) L is then substituted to the differential equation of the circuit model and i_{k+1} can be calculated by the fourth-order Runge-Kutta method.

(iii) i_{k+1} is used as a new input current to solve the new dynamic inductance at the next moment.

(iv) When the error between the excitation current i_k and i_{k+1} is less than 0.1%, it is considered that the current has reached a steady state and the iteration terminates.

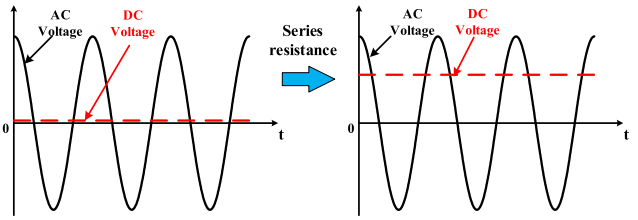

FIGURE 2. DC voltage component amplification realized by the series resistance.

B. SERIES RESISTANCE AND VOLTAGE COMPENSATION METHOD (SRVCM)

Unlike with the general transformer, the resistance of the UHV autotransformer is extremely small compared to its large inductance, especially when inductive load imposed at low voltage side. The long transient process will encounter difficulties due to the tremendous requirements of computer memory and CPU time. Beyond that, this characteristic of large inductance and small resistance could also easily lead to the miscalculations as the component of DC bias can be easily neglected by the ultra-high AC voltage in the simulation. By means of series resistance, the DC voltage can be amplified to a content, which is not easy to be neglected, as shown in Fig. 2. Therefore, the accuracy of DC bias calculation can be increased by series resistance.

In order to speed up the convergence of the transient process, a large resistance R_s is series in the circuit, as shown in Fig. 1 (c). The time to steady state of excitation current with various series resistance are shown in Fig. 3, it can be seen

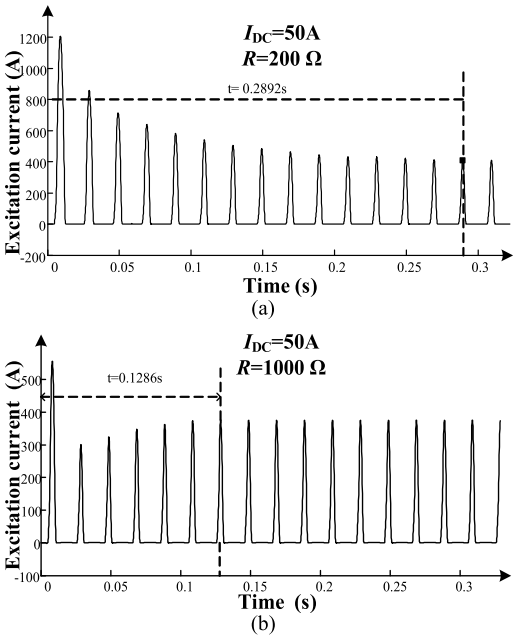

FIGURE 3. Transient process of excitation current with various series resistance. (a) Series resistance of 200 Ω. (b) Series resistance of 1000 Ω.

TABLE 1. Miscalculation with different series resistance.

I_{DC}/A	Miscalculation/%		
	200 Ω	500 Ω	1000 Ω
20	23.8	7.4	3.7
50	10.8	5.1	2.4
100	7.0	2.5	0.7

that the series resistance obviously speeds up the convergence of the transient process, from 0.2892s of 200 Ω to 0.1286s of 1000 Ω, which reduced almost 55% transient time.

The series resistance does shorten the calculation time obviously by reducing the time constant. However, as the increase of the series resistance the accuracy grow rate gradually slows down. The series resistance value should be selected according to various situations. On the one hand, the series resistance is determined by the DC bias current. As can be seen in Table. 1, with the same series resistance, different DC bias current owns different miscalculation. When series resistance is 200 Ω, the miscalculation is 23.8% and 7.0% with 20 A and 100 A, respectively. On the other hand, the side effects of the series resistance are also needed to be taken into account. The larger series resistance will cause a bigger voltage drop, which means more voltage compensation, whereas, the effects by increasing the series resistance are getting smaller. Such as when I_{DC} is 100 A, the miscalculation can drop to 2.5% with 500 Ω and only get 1.8% decrease with another 500 Ω.

In order to revise the voltage drop caused by series resistance, voltage compensation is required, the compensation steps are as follows:

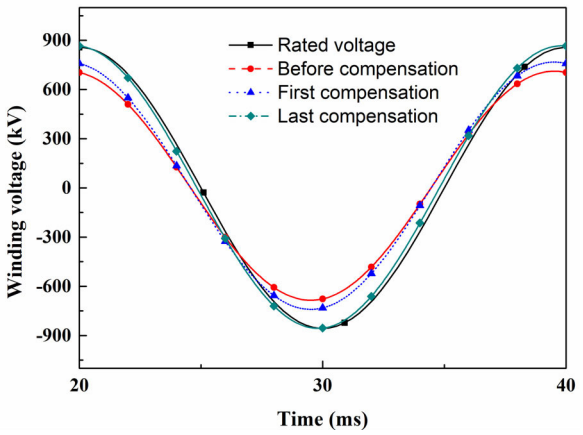

FIGURE 4. Revision of winding current u_1 by voltage compensation.

(i) Solving the k_{th} calculated winding current i_k of a full cycle in steady state.

(ii) The value of compensation voltage is equal to series resistance multiplied the difference between winding current i_k and DC component I_{kDC}.

(iii) The $k+1_{th}$ voltage compensation can be obtained by adding the compensation voltage to the original AC and DC voltage source, as shown in (9).

(iv) The compensation ends until the voltage u_1 meets the criterion, as presented in (10).

$$u_{k+1} = U_m \cos(\omega t) + U_{DC} + R(i_k - I_{kDC}) \quad k = 1, 2... \tag{9}$$

$$\max |u_1 - U_m \cos(\omega t)| \leq 1\% U_m \tag{10}$$

where u_{k+1} is the $(k+1)$ voltage supply, U_m is the amplitude of the rated AC voltage on the original side, U_{DC} is the inserted DC voltage, i_k is k_{th} current in steady state, I_{kDC} is DC component in steady state.

The winding voltage u_1 after series resistance with and without compensation are shown in Fig. 4, respectively. As shown in Fig. 4, a big voltage variation occurs before the compensation, which is the side effects of the series resistance. By the use of voltage compensation, the voltage waveform almost restored to the rated voltage.

Table 1 shows the miscalculation of DC bias calculation under various series resistance, 200 Ω, 500 Ω and 1000 Ω are in series at high voltage side under various DC bias current, respectively. In theory, the DC component of winding current should be equal to the imposed DC bias current when the winding current reached the steady state. Therefore, the accuracy of the calculation can be verified by comparing the DC component of winding current with the DC bias current. Taking $I_{DC} = 100$ A as an example, with the increase of series resistance, the DC component in the high voltage winding gradually approximates to the added DC bias current value, and its miscalculation gradually drop from 7.0% of 200 Ω to 2.5% of 500 Ω and 0.7% of 1000 Ω. It can be concluded that the series resistance can effectively improve the calculation accuracy, as shown in Table 1. And the comparison of

TABLE 2. Comparison of miscalculation between conventional and srvcm.

Method		Miscalculation with I_{DC}=20 A (%)		
		ε=1.0e-02	ε=1.0e-04	ε=1.0e-06
Conventional		94.8	24.8	17.6
SRVCM	200.0	23.8	8.8	3.5
	500.0	7.4	0.5	0.3
	1000.0	3.7	0.4	0.3

TABLE 3. Parameters of UHV transformer.

Quantity	Parameter
Type of UHV transformer	ODFPS-1000000/1000
Rated capacity (MVA)	1000/1000/334
Rated frequency (Hz)	50
Rated voltage (kV)	$\frac{1050}{\sqrt{3}}/\left(\frac{525}{\sqrt{3}}\pm 4\times 1.25\%\right)/110$
Rated current (A)	1649.57/3299.14/3036.3
High/middle/low voltage turn	1356/678/246
Core structure	2 main columns, 2 side columns

miscalculation between conventional and the SRVCM under various critical error criterion are present in Table 2. The miscalculation is obtained by comparing the DC components in the excitation current with the imposed DC bias current. As can be seen in the Table. 2, even under a strict critical error criterion like ε = 1.0e-06, the miscalculation could still reach 17.6% with conventional method, whereas, the miscalculation reaches 94.8% with the critical error criterion ε = 1.0e-02. However, by means of SRVCM, the miscalculation with 1000 Ω can drops to 3.7% with the critical error criterion ε = 1.0e-02.

III. SIMULATION OF DC BIAS EFFECTS ON UHV AUTOTRANSFORMER

This paper conducts simulation analysis for 1000 kV UHV autotransformer, and its specific parameters are presented in Table 3. By utilizing the SRVCM, the electrical quantities can be calculated with acceptable time and accuracy. The flux distribution, excitation current, and its harmonic spectrum under various DC bias are shown in Fig. 5 and Fig. 6. During the first half cycle in which the AC flux and the DC flux are in the same direction, hence the core will be saturated. As can be seen from Fig. 5 (a), the flux density of the main limb of the core is arising from 1.65T to 2.0T under 5A DC bias current. Due to the saturation the excitation current will arise greatly. Whereas, in last half cycle, the AC and DC flux are in the opposite direction, hence, the excitation current will reduce rapidly to a small value, as shown in Fig. 5 (b). As can be seen from Fig. 5 (c), the peak value of excitation current without DC bias current is 1.84 A, and the peak value increase to 194 A, 393A, 545A and 628A with 20 A, 50 A, 80 A and 100 A DC bias current, respectively. The distortion

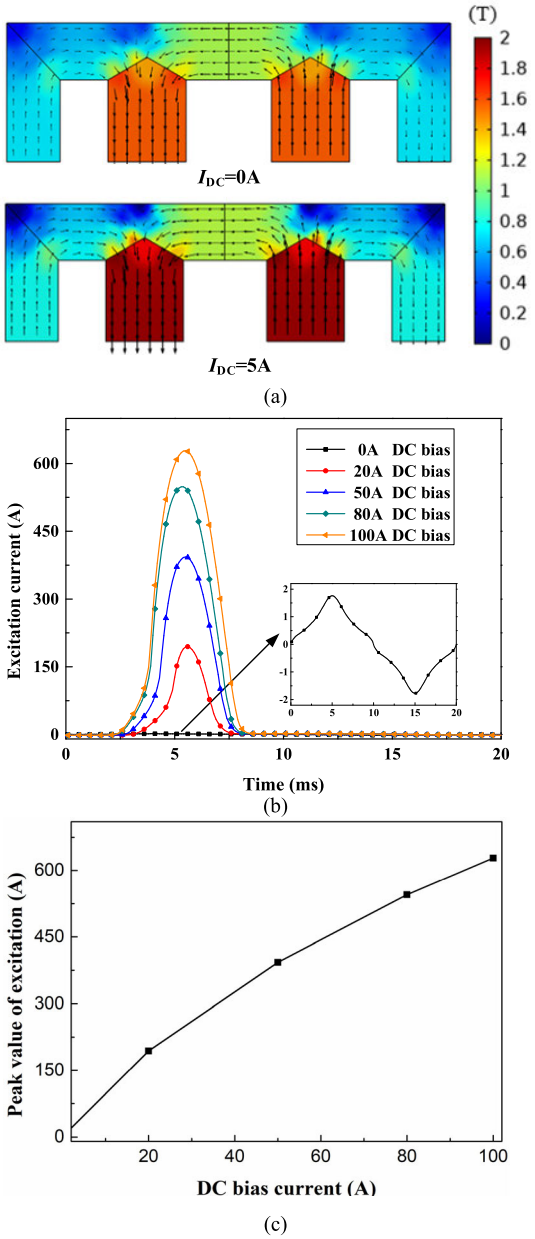

FIGURE 5. Simulation of excitation current under various DC bias current. (a) Flux distribution at 1/4 cycle. (b) Excitation current waveform. (c) Peak value increase with DC bias current.

under 100 A DC bias current is 340 times higher than the rated excitation current.

Discrete Fourier transform (DFT) is applied to the waveform of excitation current under DC bias. The harmonic magnitudes of excitation current under various DC bias currents are shown in Fig. 6. Among the harmonic frequencies, the number 0 represents the DC component, no.1 represents the fundamental component, and the other numbers represent each harmonic order. It can be seen from Fig. 6, harmonics occur and arise greatly as the DC bias current increase, and the distortion mainly concentrated before 6th harmonic. High order harmonics are less affected by the DC bias current.

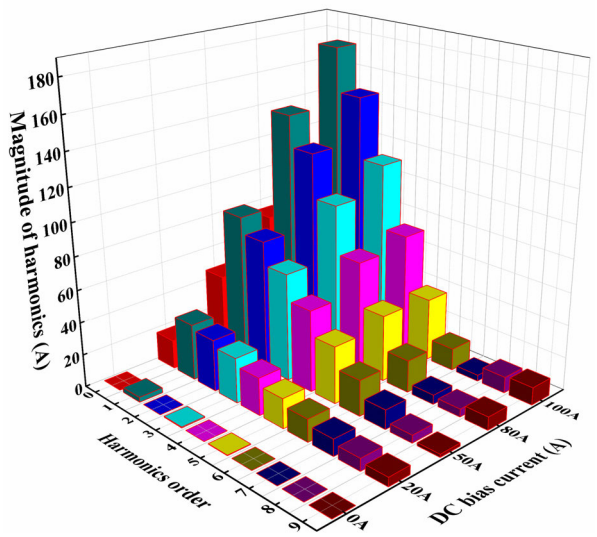

FIGURE 6. Harmonics spectrum of excitation current under various DC bias current.

By calculating and analyzing the DC bias effects on UHV transformer under no load condition, three aspects are notable:

(i) Distortion occurs mainly in the first half of the cycle, peaking in the quarter cycle, the distortion under DC bias current can be hundreds of times higher than the rated one. The excitation current in last half of the cycle is less affected by the DC bias current due to the opposite direction.

(ii) Harmonics increase greatly as DC bias current increase, even harmonics appear in excitation current harmonics, mainly the 2nd, 4th and 6th order, high order harmonics increase much slower than the low order harmonics.

(iii) The growth rate of second harmonic almost remains unchanged, whereas, the growth rate of higher harmonics gradually slows down as the DC bias current goes. This means the second harmonic could be selected as an indicator sign for monitoring the DC bias current introduced into the transformer windings.

IV. EXPERIMENTAL VALIDATION

To verify the correctness of the model, a downscaled single-phase four-column three-winding autotransformer was built with parameters of 5000 VA and 360V, which is shown in Fig. 7 (a). In order to ensure the downscaled model has the same behavior as the UHV autotransformer, its core structure and connection mode are consistent with UHV autotransformer, the downscaled model's size is 1/12 of the UHV autotransformer, whose length is 661 mm, width is 100 mm and height is 356 mm, respectively. The flux density in rated operation is 1.65 T, which is the same as the UHV autotransformer. And the ratio of turns, voltage, and capacity of each side are consistent with the UHV autotransformer. The DC bias test platform is shown in Fig. 7 (b) and (c). The voltage regulator is connected to a voltage source, providing a 360V 50Hz sinusoidal excitation to the arrangement. The isolation

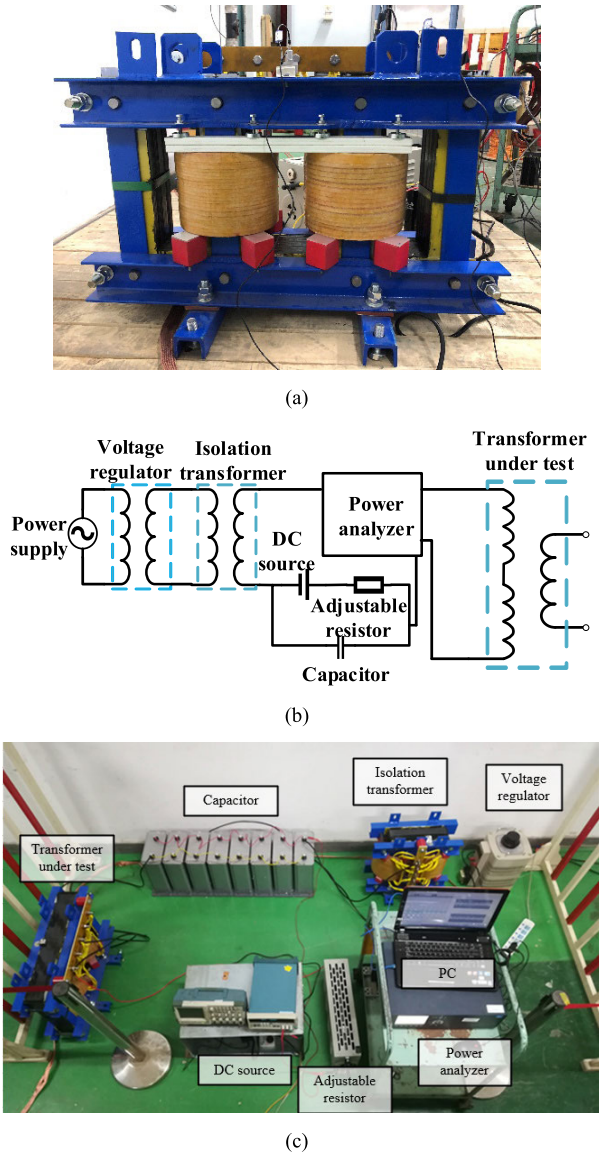

FIGURE 7. Experimental platform of a downscaled autotransformer under DC bias. (a) A downscaled transformer. (b) Schematic diagram. (c) Photo of the experimental platform.

transformer is utilized for avoiding the DC current effects on the supply source. The DC source with adjustable resistance are used to obtain various DC current while the eight parallel capacitors of 1194uF are used to reduce the AC current passing through the DC source. The electrical quantities are measured by a power analyzer. The equipment parameters in the test platform are shown in Table 4.

The DC bias no-load test of a downscaled transformer model was carried out. The measured value of no-load excitation current without DC bias current and winding current under rated operation are compared with simulation results, as shown in Fig. 8. And the comparison between the simulated and measured values of excitation current and winding current under various DC bias current is shown in Fig. 9.

TABLE 4. Equipment configuration of experimental platform.

Equipment	Parameter
Voltage Regulator	Rated capacitor:10000 VA Output voltage: 0V~300V
Isolation Transformer	Rated capacitor:10000VA, Input voltage: 360V, Output voltage: 360V
DC Source	Tektronix PWS 2326, Output DC current:0A~6A, voltage: 0V~32V
Capacitor	BSMJ-0.4-60-1, Capacitance: 8*1194μF (8 capacitors in parallel, impedance is 0.3Ω)
Power Analyzer	Fluke Norma 5000

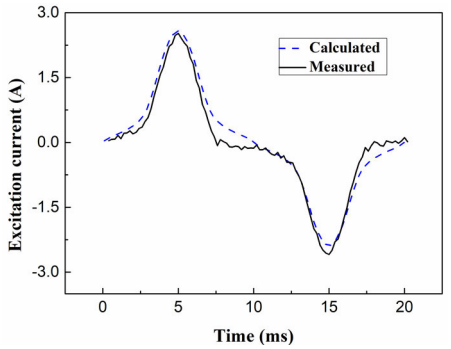

FIGURE 8. The current of calculated and measured without DC bias current.

As can be known in Fig. 9, the excitation current under DC bias current of the downscaled transformer shows the same tendency as the excitation current of UHV transformer. The results show that the relative deviations of peak value and effective value of excitation current without DC bias are 2.2% and 4.2% respectively. Taking excitation current under 5A DC bias current as an example, the relative deviations of peak excitation current and effective value under DC bias are 7.9% and 3.7%, respectively. This measured data shows a good agreement with the simulation results.

It should be noted that there are two errors can be noticed easily in Fig. 8 and Fig. 9, which are mainly caused by:

(i) Neglecting the hysteresis effects, which cause the error when excitation current close to around 0, as shown in Fig. 8.

(ii) Linear curve fitting is utilized for the deep saturation situation, as shown in Fig. 1 (b), thus the actual saturation condition is severer than the simulated one, which causes the calculation error about peak value, as shown in Fig. 9.

The comparison between the simulation results and the experimental data shows that the proposed field-circuit coupled FEM combined with SRVCM has good accuracy in calculating DC bias effects on transformer.

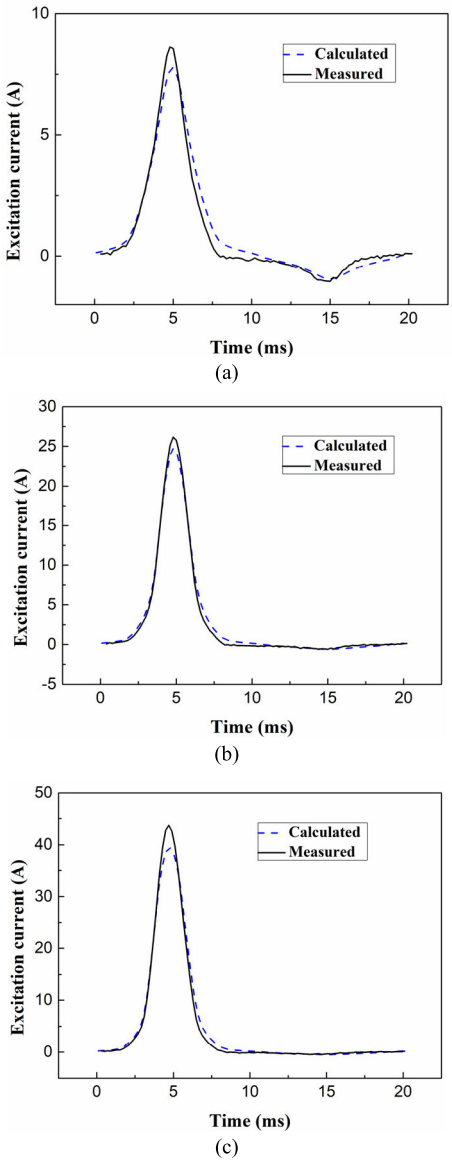

FIGURE 9. The current of calculated and measured under various DC bias current. (a) Under 1A DC bias current. (b) Under 3A DC bias current. (c) Under 5A DC bias current.

V. CONCLUSION

In this paper, a fast and accurate solution based on the time-domain field-circuit coupled FEM, combined with SRVCM is proposed. By good use of this method, the DC bias effects on UHV autotransformer without load is calculated and the distortion of excitation current under various DC bias are analyzed. By utilizing the SRVCM, it can not only speed up the convergence of the transient process due to the reduction of the time constant but also decrease the miscalculation by amplifying the order of magnitudes of DC component to the level of AC voltage source. As the increase of DC bias current, the distortion of excitation current rises sharply, mainly occurs on the first half cycle, even harmonics appear. The second harmonic almost keeps linear with DC

bias current, and other harmonics decrease with the deepening of DC biasing. The calculation error can be reduced if more data can be provided in deep saturation of the BH curve. The correctness of the proposed model is verified by a downscaled transformer.

REFERENCES

[1] D. Zhang and T. Liu, "A multi-step modeling and optimal operation calculation method for large-scale energy hub model considering two types demand responses," *IEEE Trans. Smart Grid*, vol. 10, no. 6, pp. 6735–6746, Nov. 2019, doi: 10.1109/TSG.2019.2910930.

[2] T. Liu, D. Zhang, H. Dai, and T. Wu, "Intelligent modeling and optimization for smart energy hub," *IEEE Trans. Ind. Electron.*, vol. 66, no. 12, pp. 9898–9908, Dec. 2019.

[3] T. Liu, D. Zhang, S. Wang, and T. Wu, "Standardized modelling and economic optimization of multi-carrier energy systems considering energy storage and demand response," *Energy Convers. Manage.*, vol. 182, pp. 126–142, Feb. 2019.

[4] J. Zhang, B. Li, B. Tang, J. Yang, and L. Huang, "Resistor-capacitor combined DC bias protection of AC power grid of Jiuquan-Hunan ±800 kV transmission lines," *IEEE Access*, vol. 7, pp. 38730–38737, 2019.

[5] Z. Wang, R. Tan, and Y. Zang, "DC-bias calculation for UHV transformer in no-load by series resistance," *Trans. China Electrotech. Soc.*, vol. 32, no. 8, pp. 129–137, Apr. 2017.

[6] J. He, Y. Zhou, Z. Li, and J. Yuan, "Feasibility of using one-column-varistor arresters in 1000-kV UHV substations," *IEEE Trans. Power Del.*, vol. 31, no. 4, pp. 1533–1541, Aug. 2016.

[7] G. Buticchi and E. Lorenzani, "Detection method of the DC bias in distribution power transformers," *IEEE Trans. Ind. Electron.*, vol. 60, no. 8, pp. 3539–3549, Aug. 2013.

[8] P. Picher, L. Bolduc, A. Dutil, and V. Q. Pham, "Study of the acceptable DC current limit in core-form power transformers," *IEEE Trans. Power Del.*, vol. 12, no. 1, pp. 257–265, Jan. 1997.

[9] S. Yang, G. Zhou, and Z. Wei, "Influence of high voltage DC transmission on measuring accuracy of current transformers," *IEEE Access*, vol. 6, pp. 72629–72634, 2018.

[10] L. Marti, A. Rezaei-Zare, and A. Narang, "Simulation of transformer hotspot heating due to geomagnetically induced currents," *IEEE Trans. Power Del.*, vol. 28, no. 1, pp. 320–327, Jan. 2013.

[11] X. Deng, S. Mardanikorani, G. Zhou, and J.-P.-M. G. Linnartz, "DC-bias for optical OFDM in visible light communications," *IEEE Access*, vol. 7, pp. 98319–98330, 2019.

[12] J. He, Z. Yu, R. Zeng, and B. Zhang, "Vibration and audible noise characteristics of AC transformer caused by HVDC system under monopole operation," *IEEE Trans. Power Del.*, vol. 27, no. 4, pp. 1835–1842, Oct. 2012.

[13] C. A. Baguley, U. K. Madawala, and B. Carsten, "The impact of vibration due to magnetostriction on the core losses of ferrite toroidals under DC bias," *IEEE Trans. Magn.*, vol. 47, no. 8, pp. 2022–2028, Aug. 2011.

[14] H. Pfutzner, G. Shilyashki, C. Bengtsson, G. Trenner, and E. Gerstbauer, "Effects of DC bias on regional flux and magnetostriction of a single-phase transformer core modeled by 3-D MACC," *IEEE Trans. Magn.*, vol. 54, no. 5, pp. 1–6, May 2018.

[15] T. D. Kefalas and A. G. Kladas, "Harmonic impact on distribution transformer no-load loss," *IEEE Trans. Ind. Electron.*, vol. 57, no. 1, pp. 193–200, Jan. 2010.

[16] D. Zhang, H. Dai, H. Zhao, and T. Wu, "A fast identification method for rotor flux density harmonics and resulting rotor iron losses of inverter-fed induction motors," *IEEE Trans. Ind. Electron.*, vol. 65, no. 7, pp. 5384–5394, Jul. 2018.

[17] R. Wang, W. Chen, L. Zhu, S. Ji, X. Li, L. Dai, and Y. Yang, "Modeling of acoustic emission generated by filter capacitors in HVDC converter station," *IEEE Access*, vol. 7, pp. 102876–102886, 2019.

[18] J. Wu, J. Wang, C. Gan, Q. Sun, and W. Kong, "Efficiency optimization of PMSM drives using field-circuit coupled FEM for EV/HEV applications," *IEEE Access*, vol. 6, pp. 15192–15201, 2018.

[19] W. Tong, S. Wang, S. Wu, and R. Tang, "A complete quasi-3-D analytical model of no-load magnetic field of double-sided slotted AFPMMs considering end effect," *IEEE Access*, vol. 6, pp. 59557–59566, 2018.

[20] O. Biro, G. Koczka, G. Leber, K. Preis, and B. Wagner, "Finite element analysis of three-phase three-limb power transformers under DC bias," *IEEE Trans. Magn.*, vol. 50, no. 2, pp. 565–568, Feb. 2014.

[21] D. Zhang, T. Liu, H. Zhao, and T. Wu, "An analytical iron loss calculation model of inverter-fed induction motors considering supply and slot harmonics," *IEEE Trans. Ind. Electron.*, vol. 66, no. 12, pp. 9194–9204, Dec. 2019.

[22] D. Zhang, T. Liu, C. He, and T. Wu, "A new 2-D multi-slice time-stepping finite element method and its application in analyzing the transient characteristics of induction motors under symmetrical sag conditions," *IEEE Access*, vol. 6, pp. 47036–47046, 2018.

[23] X. Zhao, Y. Zhong, O. Biro, L. Li, Z. Cheng, D. Guan, and F. Meng, "Computation and analysis of DC-biased eddy current problems by an efficient fixed-point technique in the harmonic domain," *IEEE Trans. Magn.*, vol. 51, no. 11, pp. 1–4, Nov. 2015.

[24] Z. Wang, C. Pan, and S. Zhou, "Transient magnetic circuit coupled model of transformer based on edge finite element method," *Trans. China Electrotech. Soc.*, vol. 27, no. 9, pp. 146–152, Sep. 2012.

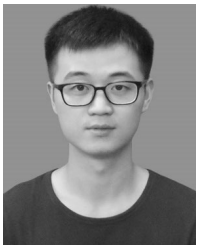

BING LI was born in Hunan, China, in 1991. He received the B.Sc. degree in electrical engineering and management from North China Electric Power University, Beijing, China, in 2014, where he is currently pursuing the Ph.D. degree in electrical engineering.

His research interests include electromagnetic computation, multiphysics coupling modeling, and DC bias effects on characteristics of vibration and acoustic noise of transformer.

ZEZHONG WANG was born in Shandong, China, in 1960. He received the bachelor's, master's, and Ph.D. degrees from the Department of Electrical Engineering, Tsinghua University, Beijing, China, in 1983, 1986, and 1989, respectively.

He is currently a Professor with the Department of Electrical and Electric Engineering, North China Electric Power University, Beijing. His research interests include electromagnetic field analysis and calculation, power system electromagnetic compatibility, and electromagnetic measurement.

SUXIN GUO was born in Shanxi, China, in 1996. He received the B.Sc. degree in power systems and automation from North China Electric Power University, Beijing, China, where he is currently pursuing the master's degree in electrical engineering.

His research interests include EMC and numerical calculation of electromagnetic fields in power systems.

MINGYANG LI was born in Henan, China, in 1991. He received the B.Sc. degree in electrical engineering and automation from the Institute of Disaster Prevention Science and Technology, Hebei, China, in 2013, and the M.Sc. degree in electrical theory and new technology from North China Electric Power University, Beijing, China, in 2016, where he is currently pursuing the Ph.D. degree in electrical engineering.

His research interests include electromagnetic field numerical calculation and electromagnetic compatibility.